Improving the Functional Control of Aged Ferroelectrics Using Insights from Atomistic Modeling

J. B. J. Chapman,[1,2] R. E. Cohen,[1,3,4] A. V. Kimmel,[1] and D. M. Duffy[1]
[1]Department of Physics and Astronomy, University College London, Gower Street, London WC1E 6BT, United Kingdom
[2]National Physical Laboratory, Hampton Road, Teddington TW11 0LW, United Kingdom
[3]Extreme Materials Initiative, Geophysical Laboratory, Carnegie Institution of Washington, Washington, D.C. 20015, USA
[4]Ludwig Maximilians University Munich, 80539 München, Germany
(Received 8 June 2017; published 24 October 2017)

We provide a fundamental insight into the microscopic mechanisms of the aging processes. Using large-scale molecular dynamics simulations of the prototypical ferroelectric material $PbTiO_3$, we demonstrate that the experimentally observed aging phenomena can be reproduced from intrinsic interactions of defect dipoles related to dopant-vacancy associates, even in the absence of extrinsic effects. We show that variation of the dopant concentration modifies the material's hysteretic response. We identify a universal method to reduce loss and tune the electromechanical properties of inexpensive ceramics for efficient technologies.

DOI: 10.1103/PhysRevLett.119.177602

Technologies utilizing ferroelectric components are ubiquitous in modern devices, being used from mobile phones, diesel engine drive injectors, and sonar, to print heads and nonvolatile memory [1–4]. Doping with transition metals has been shown experimentally to improve electromechanical properties of widely used ferroelectrics. For example, doping of $BaTiO_3$, $PbTiO_3$, $Pb(Zr_{1-x}Ti_x)O_3$ (PZT) and $_{(1-x)}Pb(Mg_{1/3}Nb_{2/3})O_3$-$_x PbTiO_3$ (PMNPT) is used to improve the functional properties and efficiency of these simple and cheap oxides [5–13]. However, the fundamental origin of the electromechanical improvements is not understood and requires full characterization to enable properties to be directly tuned for purpose and functional lifetimes to be accurately predicted.

Dopant interactions can be classified as intrinsic (bulk or volume) or extrinsic (boundary). Extrinsic coupling is associated with domain wall and grain boundary effects. Defects, including dopants and vacancies, migrate to domain walls and subsequently pin their propagation, resulting in fatigue of the material's switching properties [14]. Intrinsic effects occur independent of interaction with domain walls, as they arise due to the interaction between defect induced dipoles $\vec{p}_d$ and the spontaneous polarization of the domain surrounding the defect site $\vec{P}_s$. Strong evidence from electron paramagnetic spin resonance (ESR) and density functional theory (DFT) calculations has shown dopants or impurities, such as iron Fe^{3+} and copper Cu^{2+}, in PZT (or Mn^{2+} in $BaTiO_3$) substitute the B cations as acceptors, which bind to charge compensating oxygen vacancies V_O^{2-} to form thermodynamically stable defect complexes [15,16]. In Kröger-Vink notation, the divalent dopant-vacancy associates can be written as $(B''_{Ti} + V_O^{\bullet\bullet})^{\times}$, where B''_{Ti} is an unspecified divalent dopant substituting a Ti^{4+} site, $V_O^{\bullet\bullet}$ is an oxygen vacancy with a $+2e$ charge relative to the defect-free site, $'$ identifies a negative charge unit $(-e)$, $\bullet$ represents a positive charge unit $(+e)$, and $\times$ stands for charge neutrality. DFT calculations have shown defect dipoles $\vec{p}_d$ spontaneously form for $(Fe'_{Ti} + V_O^{\bullet\bullet})^{\bullet}$ [17] and $(Cu''_{Ti} + V_O^{\bullet\bullet})^{\times}$ [16] associates in $PbTiO_3$ and $(Mn''_{Ti} + V_O^{\bullet\bullet})^{\times}$ in $BaTiO_3$ [10,18] and the energetically favorable orientation is along the polar axis [001]. Group-IIIB and group-VB acceptor substitutes on Ti sites in $PbTiO_3$ have been shown to form immobile clusters of dopant-vacancy associates which have different structures when the associate is aligned parallel or perpendicular to the polar axis [19]. $(V''_{Pb} + V_O^{\bullet\bullet})^{\times}$ divacancy complexes in $PbTiO_3$ have been calculated to have a local dipole moment twice the bulk value [20].

It has been proposed that in aged ferroelectrics, defect dipoles produced from dopant-vacancy associates will slowly rotate to align in parallel with the domain symmetry to minimize its energy state [9,21,22]. The coalignment and correlated behavior of these aged defect dipoles has been proposed to create a macroscopically measurable internal bias, which, in turn, is responsible for experimentally observed aging phenomena, including a ten- to 40-fold increase in piezoelectric coefficients, shifts in the hysteresis along the electric field axis, and pinched or double hysteresis loops typically associated with antiferroelectrics [1,9–11].

In this Letter, we use large-scale classical molecular dynamics to model aging arising from defect dipoles of dopant-vacancy associates in tetragonal bulk lead titanate ($PbTiO_3$). We show that the experimentally observed large-signal effects (P-E and S-E hysteresis) of aged perovskite ferroelectrics, pinched and double hysteresis, shifted hysteresis, and a large recoverable electromechanical response can be reproduced from intrinsic effects alone and identify the microscopic mechanisms of each case.

We study ideal and aliovalent-doped bulk $PbTiO_3$ using molecular dynamics (MD) as implemented in the DL_POLY code [23]. We use the adiabatic core-shell interatomic

potentials derived in Gindele *et al.* [24] that reproduce the properties of bulk and thin films of $PbTiO_3$ in excellent agreement with DFT calculations [24,25]. $PbTiO_3$ has been chosen as it has a single ferroelectric phase, which reduces competing effects and because it is a parent compound for two of the most widely used ferroelectric materials in industry (PZT/PMNPT).

In this Letter, we investigate volume effects; therefore, three-dimensional periodic boundary conditions are implemented to mimic an infinite crystal devoid of surfaces, interfaces, and grain boundaries. We choose a supercell constructed from $12 \times 12 \times 12$ unit cells, approximately 125 nm^3, corresponding to 8640 atoms (for the ideal bulk). This system size is large enough for ensemble sampling but sufficiently small to prevent the formation of 90° domain walls. We use the smooth particle mesh Ewald summation for the calculation of Coulomb interactions. Coupling between strain and polarization is enabled using the constant-stress Nosé-Hoover ($N\sigma T$) ensemble with thermostat and barostat relaxation times of 0.01 and 0.1 ps, respectively. A 0.2 fs time step is used in all instances.

We calculate polarization-electric field (P-E) hysteresis using a quasistatic approach. Starting at 0 kV/mm, the electric field is cycled between the limits ±150 kV/mm in 16.7 kV/mm intervals. For each field strength, the system is restarted using the coordinates, velocities, and forces from the previous calculation and equilibrated for 4 ps to enable the system to equilibrate following the E-field impulse. This is followed by an 8 ps production run over which statistics are collected (total of 12 ps per iteration). This approach is advantageous over a continuous hysteresis which requires a shallow gradient for the electric field, large simulation sizes, and very long run times to achieve similar accuracy. We calculate the local polarization by considering conventional Ti-centered unit cells as implemented in Refs. [24–26]. Further details are provided in the Supplemental Material [27].

A dopant-vacancy concentration $n_d = 100(N_{\mathrm{Ti}}^{\mathrm{ideal}} - N_{B''})/N_{\mathrm{Ti}}^{\mathrm{ideal}}$ is introduced into the supercell initially containing $N_{\mathrm{Ti}}^{\mathrm{ideal}}$ Ti atoms by randomly selecting a total of $N_{B''}$ Ti atoms to be replaced with generic divalent dopants B''_{Ti}. Each dopant is coordinated by six nearest neighboring oxygen sites from which a charge compensating oxygen vacancy $V_{\mathrm{O}}^{\bullet\bullet}$ can be introduced. This configuration mimics $(B''_{\mathrm{Ti}} + V_{\mathrm{O}}^{\bullet\bullet})^{\times}$ dopant-vacancy associates observed from ESR experiments [Fig. 1(a)]. In experiments it is observed that the properties of an aged sample can be removed by heating above the Curie temperature for a long period and then rapidly quenching. It has been hypothesized that during this "unaging" process in the cubic phase of the prototype ferroelectric, each orientation of the defect dipole is equally probable such that vacancies will thermally hop between the neighboring oxygen site adjacent to the dopant and eventually 1/6 defect dipoles will populate each of the six possible directions [9]. These are then frozen when quenched into the ferroelectric phase. Ferroelectrics can then be intentionally aged again by applying a bias field for a significantly long period. Even in the absence of an aging field, defect dipoles in a sample left for a long period will align with the spontaneous polarization of the domain [11]. When constructing the supercell for a particular simulation, the choice of which oxygen is removed neighboring the dopant depends on the aged or unaged condition: (1) Unaged condition. To simulate unaged tetragonal $PbTiO_3$, we assign $N_{B''}/6$ defect dipoles along each of the six possible orientations causing the total moment to cancel; see Fig. 1(b). (2) Aged condition. To simulate an aged $PbTiO_3$ sample, each $V_{\mathrm{O}}^{\bullet\bullet}$ is selected to situate on the oxygen site along the aging direction (defined below) relative to its associated dopant. We arbitrarily choose the aging direction along $+\hat{x}$ [see Fig. 1(a)]. This initializes all defect dipoles $\vec{p}_d$ as parallel, polarized along $[\bar{1}00]$ as shown in Fig. 1(c).

The aging direction is defined relative to the driving field for the hysteresis characterization. If the defect dipoles are coaligned with the driving field, we label this as aged(∥) [Fig. 1(d)], whereas perpendicular alignments are labeled aged(⊥) [see Fig. 1(e)]. The strain is calculated as $\Delta\epsilon = (c_0 - c)/c$, where c_0 is the relaxed lattice constant (parallel to the drive field orientation) under no applied field.

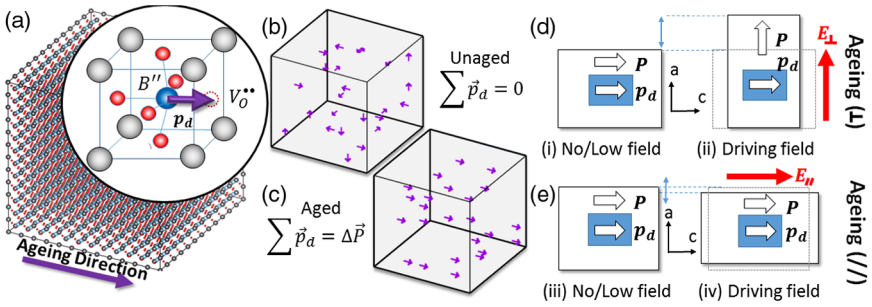

FIG. 1. System configuration for MD simulations of aging. (a) $PbTiO_3$ supercell including defect dipoles from $(B''_{\mathrm{Ti}} + V_{\mathrm{O}}^{\bullet\bullet})^{\times}$ associates (inset). (b) Defect dipoles in unaged $PbTiO_3$ are randomly orientated. (c) Aged $PbTiO_3$ is modelled by aligning all defect dipoles along the aging direction [100]. (d) Schematic of perpendicular aging. A [001] poling field is applied perpendicular to the aging orientation. (e) Schematic of parallel aging. The poling field is applied parallel to the aging orientation.

First, we discuss the results obtained at 100 K to observe the ideal behavior without thermal diffusion or hopping [28,29]. The calculated *P-E* hysteresis of $PbTiO_3$ in response to an external driving field is shown in Fig. 2(a) for the defect-free bulk, unaged and the two aged conditions. Each curve consists of a single quasistatic loop for a configuration with randomly distributed sites of the dopant substitutions. Consistency of the hysteresis has been checked for a sample of different input configurations. In all instances, the response is highly nonlinear, typical of ferroelectrics. For the ideal bulk case, a symmetric, square loop indicative of a hard ferroelectric is observed. We note our bulk coercive field E_c^{int} corresponds to the material's intrinsic coercive field, which greatly exceeds those measured experimentally for Pb-based ferroelectrics [2]. This is because our model excludes grain boundaries, surfaces, and domain walls which would all act as nucleation sites, which lower the energy barrier for reversal in physical samples. Our result of 130 kV/mm matches other MD models [30] and is in excellent agreement with the intrinsic coercive field of 150 kV/mm calculated using density functional perturbation theory [31].

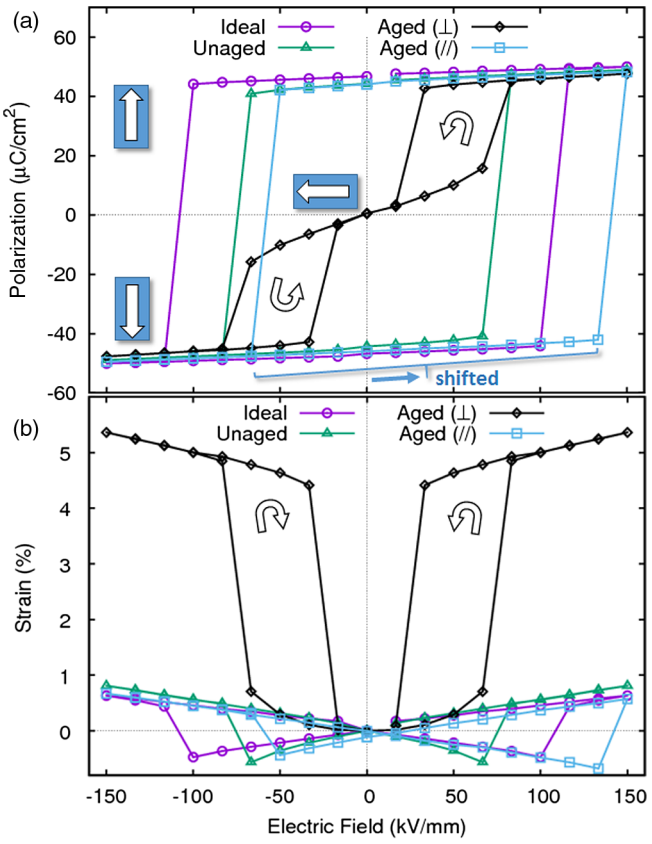

FIG. 2. Hysteresis of doped $PbTiO_3$ when defect-free (purple circles), unaged (green triangles), poled parallel to the aged orientation (blue squares), and aged perpendicular to the poling direction (black diamonds). (a) Polarization-electric field hysteresis. (b) Electrostrain hysteresis.

Figure 2(a) shows the hysteresis of an aged single domain simulated sample, with a defect concentration of 1.38%, in response to a driving field perpendicular to the direction in which the material was aged. Interestingly, when the system is equilibrated with no applied field, the spontaneous polarization $\vec{P}$ reorientates parallel to the aging direction [see the Supplemental Material [27] Fig. 3 and the cartoon schematic in Fig. 1(d)]. This shows the internal bias created from the defect dipoles is sufficient to overcome the switching barrier [22]. This observation provides direct evidence supporting the work of Zhang *et al.* [11] who observed that nonswitching defect dipoles from $((Mg''_{Ti} - V^{\bullet\bullet}_O)^{\times}$ associates in $BaTiO_3$ create restoring forces that promote reversible domain switching. Under the application of the perpendicular driving field, there is an almost linear response until 67 kV/mm ($\approx E_c^{\text{int}}/2$), at which point the field strength is sufficient to switch the polarization parallel to the drive field. As the electric field decreases to zero, the polarization again reorientates along the aging axis such that no remnant polarization P_r remains in the poling direction. Thus, in our work, the iconic double hysteresis indicative of aged ferroelectrics is observed without the requirement of either domain walls or grain boundaries [1,9].

When poling parallel to the aging orientation [Fig. 1(e)], the system exhibits a shifted hysteresis curve along the electric field axis as shown in Fig. 2(a). Such an effect is well documented in the literature when there is a preferred orientation of the defect dipoles in the poling direction [14,21,32].

In the unaged simulation, we observe a symmetric square *P-E* hysteresis loop [Fig. 2(a)]. The computed coercive field of the unaged $PbTiO_3$ is reduced relative to the ideal bulk value by 35% ($0.65E_C^{\text{int}}$). The reduction of the coercive field from E_c^{int} occurs because the dopant-vacancy associates break local symmetry creating localized areas where the activation energy for nucleation of reverse domains is reduced [33].

The electrostrain (*S-E*) of each condition is shown in Fig. 2(b). Symmetric butterfly *S-E* curves are observed for both the ideal ($n_d = 0\%$) and unaged ($n_d = 1.38\%$) simulations, in excellent agreement with unaged ferroelectrics measured by experiment [2,34,35]. To test the validity of the results in comparison to experiment, we calculate the d_{33} piezoelectric tensor coefficient of bulk $PbTiO_3$ using a fluctuation-perturbation theory approach [36] and second derivative matrices using the GULP package [37] (see the Supplemental Material [27] for further details). We find $d_{33} = 47 \pm 1$ pC/N from the fluctuations and 49 pC/N from the derivatives, which agree with each other and agree well with values measured on polycrystalline $PbTiO_3$ films (52–65 pC/N) [38].

Aging parallel to the poling field is shown to induce an asymmetric *S-E* hysteresis [Fig. 2(b)]. Instances of large asymmetric *S-E* loops have been experimentally reported in a range of ferroelectric materials [39]. In Ref. [40], the

authors report a strain difference of 0.15% in Li-doped $(Bi_{0.5}Na_{0.4}K_{0.1})_{0.98}Ce_{0.2}TiO_3$ ceramics which they propose is due to alignment of $(Li_{Ti}''' - V_O^{\bullet\bullet})'$ associates. Using our prototypical system, we provide evidence that the asymmetry is likely to arise from an excess orientation along the poling direction and is a general feature of aging that may be exploited for technological applications.

It has been observed that aging of doped $BaTiO_3$ is capable of producing a large recoverable nonlinear electric field induced strain of 0.75%, far greater than those measured in PZT or PMNPT [9,10]. It is argued that a strong restoring force from aligned defect dipoles enables polar axis rotation parallel to the defect dipoles enabling reversible switching of 90° domains and could lead to the realization of strain values of 6% in $PbTiO_3$. In Fig. 2(b), we show that aging perpendicular to a poling field in $PbTiO_3$ leads to a large recoverable strain in excess of 4.5% (black diamonds). This large nonlinear strain arises from the reorientation of the polar axis along the aging direction due to the internal bias from the defect dipoles at subswitching fields (see the Supplemental Material [27] Fig. 3) $c \rightarrow a$, $\Delta\epsilon = (c_0 - a)/a$. Observing the switching behavior, we find that in this instance, the 90° switching occurs via near-homogeneous polarization rotation over a small field range rather than nucleation and growth of 90° domains—a switching mechanism predicted in bulk $PbTiO_3$ [30] and $BaTiO_3$ [22]. Therefore, we further show the volume effect of the dopant-vacancy associates to be the fundamental cause of this aging phenomenon, and a domain wall mechanism is not required for the full reproduction of experimental observations. Our aging results are in excellent agreement with a complementary bond valence model study of aging in ideal $BaTiO_3$ using fixed dipoles introduced into the crystal structure [41].

The results of an investigation into the effect of temperature on the aging phenomenon in $PbTiO_3$ are shown in Fig. 3(a) for $n_d = 1.38\%$ in the range from 50 to 400 K. As the temperature increases, a decrease in the effective coercive field and saturation polarization are observed, corresponding to a narrowing of the double hysteresis as indicated by the trend arrows. This is analogous to the behavior known for the square loop of the ideal prototype. Near room temperature under poling fields comparable to E_c, vacancy hopping becomes thermally activated causing limited events whereby a subset of defect dipoles reorientate. This was observed by tracking the displacement of each oxygen atom relative to its initial position. This reorientation can create asymmetric loops as seen at 400 K ($0.67T_c$), clearly demonstrating that at high temperatures or large fields the defect dipoles can readily realign, elucidating the microscopic mechanism for aged → unaged transitions. No defect dipoles were observed to switch below 300 K ($0.5T_c$). At 300 K, a single hopping event was observed (1/24 vacancies) and two (1/12 vacancies) at 400 K over the full hysteresis. We note that due to the relatively short simulation times, these hopping frequencies will be undersampled for accurate statistics and will be an interesting subject for future investigation.

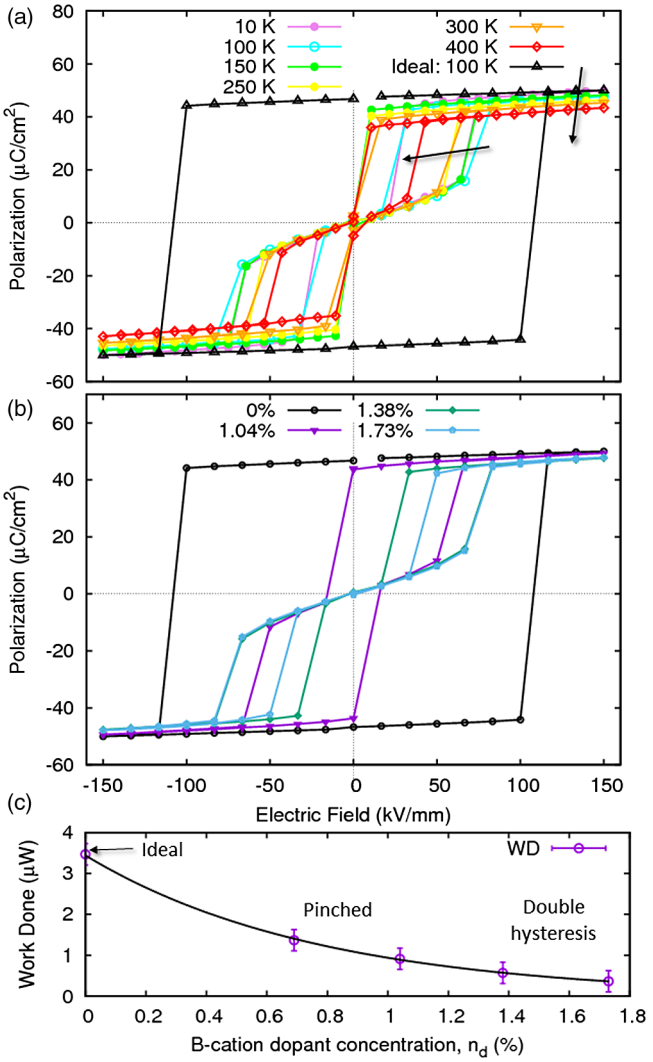

FIG. 3. Aged hysteresis properties. (a) Temperature dependence of the P-E hysteresis for $n_d = 1.38\%$. (b) The effect of dopant concentration on the hysteresis of $PbTiO_3$. Low concentrations retain the square loop of the pure ferroelectric. Pinching is observed at dopant concentrations greater than 0.78% which close to form double hysteresis loops with further increases in concentration (≈1.38%). (c) Work done to create hysteresis over a period T (area enclosed in the loop $W = (1/T)\oint EdP$). A solid line is plotted to guide the eye.

Defect concentrations close to and above 1.38% are shown to form closed double hysteresis loops described previously [Fig. 3(b)]. As the concentration is increased, the enclosed area of the hysteresis loops decreases due to the increased strength of the internal bias, which lowers the barrier for the reorientation of the polar axis. For intermediate defect concentrations (0.78% in this model), we find pinched hysteresis loops are produced. This form of P-E loop is the most common large-signal observation

noted in experimental studies of aged ferroelectrics [2,32,42]. We find that the work dissipated (area enclosed by the *P*-*E* loop) decreases with the dopant level [Fig. 3(c)]. Increased defect concentrations start to pinch the square loop which, upon further increases, leads to a closed double hysteresis and gradual reduction of area. Thus, the dissipated energy losses, effective coercive fields, and hysteretic behavior of ferroelectric materials can be controlled by varying the applied fields and dopant levels. We note that in our study we are limited by the constraint of zero total dipole moment in our unaged simulation cell, which restricts the number of dopants $N_{B''}$ to factors of 6. Thus, the concentrations identifying pinching and double hysteresis are, in fact, upper bounds.

In conclusion, we use molecular dynamics to model aging in boundary-free single domain doped $PbTiO_3$. We show that all the large-signal characteristics of aging—pinched or double hysteresis, hysteresis shifts, and large recoverable nonlinear strains—can be reproduced from intrinsic effects of defect dipoles from dopant-vacancy associates alone resulting from the net defect dipole orientation with respect to the poling field. Varying the concentration of dopants is found to modify the material's hysteretic response, suggesting a mechanism for tuning ferroelectric and electromechanical properties for enhanced device performance. This work identifies and clarifies the microscopic mechanisms involved the aging phenomena and suggests practical methods to inexpensively improve functional performance of ferroelectric ceramic based technologies.

Funding was provided by the EPSRC (Grant No. EP/G036675/1) via the Centre for Doctoral Training in Molecular Modelling and Materials Science at University College London and the National Measurement Office of the UK Department of Business Innovation and Skills. Computer services on Archer were provided via membership of the UK's HPC Materials Chemistry Consortium funded by EPSRC (Grant No. EP/L000202). We acknowledge the use of the UCL facilities LEGION and GRACE and computational resources at the London Centre for Nanotechnology. R. E. C. acknowledges support of the U.S. Office of Naval Research, the ERC Advanced grant ToMCaT, and the Carnegie Institution for Science.

[1] Y. A. Genenko, J. Glaum, M. J. Hoffman, and K. Albe, Mechanisms of aging and fatigue in ferroelectrics, Mater. Sci. Eng. B **192**, 52 (2015).
[2] J. Glaum, Y. A. Genenko, H. Kungl, L. A. Schmitt, and T. Granzow, De-aging of Fe-doped lead-zirconate-titanate ceramics by electric field cycling: 180° vs. non-180° domain wall processes, J. Appl. Phys. **112**, 034103 (2012).
[3] J. Scott and C. Paz de Araujo, Ferroelectric memories, Science **246**, 1400 (1989).
[4] G. Catalan, J. Seidel, R. Ramesh, and J. Scott, Domain wall nanoelectronics, Rev. Mod. Phys. **84**, 119 (2012).
[5] H. Neumann and G. Arlt, Dipole orientation in Cr-modified $BaTiO_3$ ceramics, Ferroelectrics **76**, 303 (1987).
[6] G. Arlt and H. Neumann, Internal bias in ferroelectric ceramics: origin and time-dependence, Ferroelectrics **87**, 109 (1988).
[7] X. Ren and K. Otsuka, Origin of rubber-like behaviour in metal alloys, Nature (London) **389**, 579 (1997).
[8] X. Ren and K. Otsuka, Universal Symmetry Property of Point Defects in Crystals, Phys. Rev. Lett. **85**, 1016 (2000).
[9] X. Ren, Large electric-field-induced strain in ferroelectric crystals by point-defect-mediated reversible domain switching, Nat. Mater. **3**, 91 (2004).
[10] L. X. Zhang and X. Ren, In situ observation of reversible domain switching in aged Mn-doped $BaTiO_3$ single crystals, Phys. Rev. B **71**, 174108 (2005).
[11] L. Zhang, E. Erdem, X. Ren, and R.-A. Eichel, Reorientation of $(Mn''_{Ti} - V_O^{\cdot\cdot})^{\times}$ defect dipoles in acceptor-modified $BaTiO_3$ single crystals: An electron paramagnetic resonance study, Appl. Phys. Lett. **93**, 202901 (2008).
[12] S. Wu, L. Wang, L. Chen, and X. Wang, Dipole orientation in Cr-modified $BaTiO_3$ ceramics, J. Mater. Sci. Mater. Electron **19**, 505 (2008).
[13] P. Perez-Delfin, J. García, D. A. Ochoa, R. Pérez, F. Guerrero, and J. A. Eiras, Effect of Mn-acceptor dopant on dielectric and piezoelectric responses of lead lanthanum zirconate titanate piezoceramics, J. Appl. Phys. **110**, 034106 (2011).
[14] K. Carl and K. H. Härdtl, Electrical aftereffects in $Pb(Ti, Zr)O_3$ ceramics, Ferroelectrics **17**, 473 (1977).
[15] P. Erhart, R. A. Eichel, P. Träskelin, and K. Albe, Association of oxygen vacancies with impurity metal ions in lead titanate, Phys. Rev. B **76**, 174116 (2007).
[16] Rudiger-A. Eichel, P. Erhart, P. Träskelin, K. Albe, H. Kungl, and M. J. Hoffman, Defect-dipole Formation in Copper-doped $PbTiO_3$ ferroelectrics, Phys. Rev. Lett. **100**, 095504 (2008).
[17] H. Meštrić, R.-A. Eichel, T. Kloss, K.-P. Dinse, So. Laubach, St. Laubach, P. C. Schmidt, K. A. Schönau, M. Knapp, and H. Ehrenberg, Iron-oxygen vacancy defect centers in $PbTiO_3$: Newman superposition model analysis and density functional calculations, Phys. Rev. B **71**, 134109 (2005).
[18] J. F. Nossa, I. I. Naumov, and R. E. Cohen, Effects of manganese addition on the electronic structure of $BaTiO_3$, Phys. Rev. B **91**, 214105 (2015).
[19] Z. Zhang, P. Wu, L. Lu, and C. Shu, Defect and electronic structures of acceptor substituted lead titanate, Appl. Phys. Lett. **92**, 112909 (2008).
[20] E. Cockayne and B. P. Burton, Dipole moment of a Pb-O vacancy pair in $PbTiO_3$, Phys. Rev. B **69**, 144116 (2004).
[21] P. V. Lambeck and G. H. Jonker, The nature of domain stabilization in ferroelectric perovskites, J. Phys. Chem. Solids **47**, 453 (1986).
[22] A. V. Kimmel, P. M. Weaver, M. G. Cain, and P. V. Sushko, Defect-mediated Lattice Relaxation and Domain Stability in Ferroelectric Oxides, Phys. Rev. Lett. **109**, 117601 (2012).
[23] I. T. Todorov, W. Smith, K. Trachenko, and M. T. Dove, DLPOLY 3: new dimensions in molecular dynamics simulations via massive parallelism, J. Mater. Chem. **16**, 1911 (2006).

[24] O. Gindele, A. Kimmel, M. G. Cain, and D. Duffy, Shell model force field for lead Zirconate Titanate $Pb(Zr_{1-x}Ti_x)O_3$, J. Phys. Chem. C **119**, 17784 (2015).

[25] J. B. J. Chapman, A. V. Kimmel, and D. M. Duffy, Novel high-temperature ferroelectric domain morphology in $PbTiO_3$ ultrathin films, Phys. Chem. Chem. Phys. **19**, 4243 (2017).

[26] M. Sepliarsky and R. E. Cohen, First-principles based atomistic modeling of phase stability in PMN-xPT, J. Phys. Condens. Matter **23**, 435902 (2011).

[27] See Supplemental Material at http://link.aps.org/supplemental/10.1103/PhysRevLett.119.177602 for further details regarding the computational calculation of related properties from the MD simulation including polarization and piezoelectric coefficients, as well as a supporting figure to complement the perpendicular aging results presented in this Letter.

[28] M. I. Morozov and D. Damjanovic, Charge migration in $Pb(Zr, Ti)O_3$ ceramics and its relation to ageing, hardening, and softening, J. Appl. Phys. **107**, 034106 (2010).

[29] D. M. Smyth, Ionic transport in ferroelectrics, Ferroelectrics **151**, 115 (1994).

[30] X. Zeng and R. E. Cohen, Thermo-electromechanical response of a ferroelectric perovskite from molecular dynamics simulations, Appl. Phys. Lett. **99**, 142902 (2011).

[31] N. Sai, K. M. Rabe, and D. Vanderbilt, Theory of structural response to macroscopic electric fields in ferroelectric systems, Phys. Rev. B **66**, 104108 (2002).

[32] T. Rojac, S. Drnovsek, A. Bencan, B. Malic, and D. Damjanovic, Role of charged defects on the electrical and electromechanical properties of rhombohedral $Pb(Zr, Ti)O_3$ with oxygen octahedra tilts, Phys. Rev. B **93**, 014102 (2016).

[33] M. Vopsaroiu, J. Blackburn, M. G. Cain, and P. M. Weaver, Thermally activated switching kinetics in second-order phase transition ferroelectrics, Phys. Rev. B **82**, 024109 (2010).

[34] N. Balke, T. Granzow, and J. Rödel, Degradation of lead-zirconate-titanate ceramics under different dc loads, J. Appl. Phys. **105**, 104105 (2009).

[35] L. X. Zhang, W. Chen, and X. Ren, Large recoverable electrostrain in Mn-doped $(Ba, Sr)TiO_3$ ceramics, Appl. Phys. Lett. **85**, 5658 (2004).

[36] A. Garcia and D. Vanderbilt, Electromechanical behavior of $BaTiO_3$ from first principles, Appl. Phys. Lett. **72**, 2981 (1998).

[37] J. D. Gale, GULP: A computer program for the symmetry-adapted simulation of solids, J. Chem. Soc., Faraday Trans. **93**, 629 (1997).

[38] Z. Kighelman, D. Damjanovic, M. Cantoni, and N. Setter, Properties of ferroelectric $PbTiO_3$ thin films, J. Appl. Phys. **91**, 1495 (2002).

[39] Y. Q. Tan, J. L. Zhang, and C. L. Wang, Aging behaviours of CuO modified $BaTiO_3$ ceramics, Adv. Appl. Ceram. **113**, 223 (2014).

[40] J. Shi, H. Fan, X. Liu, and Q. Li, Defect-dipole alignment and strain memory effect in poled Li doped $(Bi_{0.5}Na_{0.4}K_{0.1})_{0.98}Ce_{0.02}TiO_3$ ceramics, J. Mater. Sci. Mater. Electron **26**, 9409 (2015).

[41] S. Liu and R. E. Cohen, Multiscale simulations of defect dipole-enhanced electromechanical coupling at dilute defect concentrations, Appl. Phys. Lett. **111**, 082903 (2017).

[42] M. I. Morozov and D. Damjanovic, Hardening-softening transition in Fe-doped $Pb(Zr, Ti)O_3$ ceramics and evolution of the third harmonic of the polarization response, J. Appl. Phys. **104**, 034107 (2008).